Characterization of Retrogression and Reaging Behavior of 8090 Al-Li-Cu-Mg-Zr Alloy

K.S. GHOSH, K. DAS, and U.K. CHATTERJEE

An 8090 Al-Li-Cu-Mg-Zr alloy in the peak-aged (T8) temper was subjected to retrogression treatment at temperatures above and below the δ' (Al_3Li) solvus line and immediately reaged to various tempers. Retrogression and reaging (RRA) behavior is characterized by hardness testing, tensile testing, transmission electron microscopy (TEM), X-ray diffraction (XRD), differential scanning calorimetry (DSC), and electrochemical polarization studies. Retrogression of the T8 temper alloy causes dissolution primarily of δ' (Al_3Li) precipitates into solid solution that results in a decrease of hardness and tensile strength and an increase of ductility of the alloy. Reaging of the retrogressed state causes reprecipitation of the δ' precipitates in the matrix resulting in the restoration of strength and ductility properties. Retrogression and reaging to the peak-aged temper, designated at T77 temper, has been found to retain the strength of the conventional T8 temper, but with the gross aging time in the RRA temper almost twice that of the conventional T8 temper, the microstructure of the RRA temper approaches that of the overaged (T7) temper. Thus, RRA treatment contributes to an improvement of stress corrosion cracking (SCC) resistance over the conventional T8 temper while retaining the mechanical properties of T8 temper.

I. INTRODUCTION

ALUMINUM alloys containing lithium are candidate alloys for aerospace industries because of their reduction in density, increase in elastic modulus, and increase in specific strength over the most widely used conventional aluminum-base alloys.[1,2,3] The mechanical properties of Al-Li alloys are strongly sensitive to processing conditions, and therefore, product quality is more difficult to control than for conventional alloys. Al-Li alloys have unattractive fracture behavior, especially poor ductility, compared to the traditional high-strength alloys and high anisotropy of nonrecrystallized products. Moreover, these alloys, such as 2xxx and 7xxx series alloys, are also susceptible to stress corrosion cracking (SCC) in their maximum strength peak aged, T6, or T8 temper. Overaging (T7) temper has an acceptable SCC resistance, but lower strength.[4,5]

A nonconventional two-stage heat-treatment process, retrogression and reaging (RRA), identified by T77 designation, was developed by Cina.[6] The RRA treatment applied to 7xxx series has been reported to improve the SCC resistance, which makes the heat treatment attractive to the aerospace industries.[6,7] The low ductility and toughness of binary Al-Li alloys can be traced to many concurrent and mutually competitive factors, mainly the inhomogeneous nature of slip resulting from coherent matrix strengthening ordered spherical δ' precipitates and the presence of coarse equilibrium δ precipitates at the grain boundaries.[1] However, for commercial Al-Li-Cu-Mg-Zr alloys, the presence of Zr, Mg, and Cu causes precipitation of β' (Al_3Zr) dispersoids and semicoherent/incoherent T_1 (Al_2CuLi), S, and S′ (Al_2CuMg) precipitates. These precipitates result in better slip homogenization and has been found to improve ductility and fracture toughness.[8–11] Further, the ductility parameters in these alloys could also be improved by suitable heat treatments such as by thermomechanical treatments as well as by proper RRA treatments. Hence, the principal benefits of RRA treatments are increased reliability, reduced maintenance costs, and avoidance of weight penalties by the use of standard overaged temper.

Extensive work has been done on 7xxx series alloys to optimize the heat-treatment conditions in RRA treatments[12] and to study the effects of RRA on microstructural changes and precipitation behavior,[13,14,15] dislocation densities,[16,17] physical and strength properties,[18,19] and finally on SCC behaviour.[15,20–23] A similar type of work has also been initiated on Al-Li alloys and the results show that RRA treatment increases SCC resistance and exfoliation corrosion resistance.[24–28] However, little work is reported on the characterization of RRA behavior on 8xxx series Al-Li-Cu-Mg-Zr alloys. In the present work, characterization of RRA behavior of the 8090 Al-Li-Cu-Mg-Zr base alloy by various techniques, *viz.* hardness and tensile testing, transmission electron microscopy (TEM), X-ray diffraction (XRD), differential scanning calorimetry (DSC), electrochemical polarization studies, and measurement of electrical conductivity values has been carried out and the results are discussed.

II. EXPERIMENTAL PROCEDURES

A. *Material*

The 8090 alloy was obtained from DMRL (Hyderabad, India) in sheet form having a thickness of 2.8 mm. The alloy sheet was solutionized at 530 °C to 535 °C, water quenched, stretched 1.5 to 2.5 pct, and artificially aged at 170 °C for 24 hours corresponding to the peak-aged, T8 temper. The chemical composition (weight percent) of the alloy is given in Table I.

K.S. GHOSH, Assistant Professor, is with the Department of Metallurgical and Materials Engineering, National Institute of Technology, Warangal–506 004, India. Contact e-mail: ghosh@nitw.ernet.in K. DAS, Associate Professor, and U.K. CHATTERJEE, Professor, are with the Department of Metallurgical and Materials Engineering, Indian Institute of Technology, Kharagpur–721 302, India.

Manuscript submitted September 30, 2003.

B. *RRA Heat Treatment*

Coupons of approximate dimensions $10 \times 10 \times 2.5$ mm^3 for the studies of hardness, TEM, DSC, XRD, and electrochemical polarization, and tensile specimens of approximate dimensions 25-mm gage length, 4-mm width, and 2.5-mm thickness (transverse to rolling direction) for electrical resistivity measurement and tensile testing, were obtained from the as-received alloy sheet. Retrogression treatments were applied to all of the specimens of the as-received T8 temper in a vertical tube furnace in air. The retrogression temperatures were chosen above and below the matrix strengthening precipitate δ' solvus line of the Al-Li system.[29] The specimens were retrogressed for a precise time in the furnace and quenched into ice-cold water followed by isothermal and duplex reaging to the peak-aged temper. The retrogression schedule applied to the specimens is given in Table II.

C. *Testing and Characterization Techniques*

Before testing, the specimen surface was ground to the extent of 100 μm to remove the lithium- and magnesium-depleted zones and subsurface porosity zones developed during solutionization of the alloy, which was carried out at a temperature of 530 °C to 535 °C in air.[30] The surface was ground on emery papers lubricated with kerosene oil up to 600 grits and finally deoiled. The hardness values were measured using a Vickers hardness testing machine. Tensile testing was carried out on sheet specimens having dimensions of 25-mm extended gage length, 4-mm width, and 2.6-mm thickness, using Shimadzu Autograph universal testing machine at a crosshead speed of 2 mm/min. Origin 6.1 software was used to plot the stress strain curves, importing the load and stroke data recorded in the computer of the universal testing machine. Hence, the total elastic strain in the stress strain might include a small amount of elastic strain of the gripping portion of the specimen, and thus, the elastic strain values could be on the higher side. Tests were repeated to confirm the results and the variation were within 5 pct of the reported results.

For TEM studies, the samples were mechanically thinned to a thickness of approximately 100 μm, punched to obtain 3-mm disc, and finally thinned down to perforation using a Fischione twin-jet electropolisher, operating at 25 V and 2.5 A current, in an electrolyte of composition 30 pct HNO_3 and 70 pct CH_3COOH at a temperature of approximately −20 °C. A PHILIPS* CW12 transmission electron microscope was used for the observation of the microstructures. X-ray diffraction study was carried using a PHILIPS PW 1710 diffractometer unit with cobalt and copper targets. Differential scanning calorimetry runs were initiated from room temperature to 540 °C temperature at a heating rate of 10 °C/min in an argon atmosphere, using a Stanton Redcroft model STA 625 (heat flux type) simultaneous thermal analyzer. Specimens of approximately 30 mg were cut from coupons of various tempers of the alloy and the sides of the specimens were made absolutely flat and smooth for a good contact with the crucible during the DSC runs. The output, *viz.* the neat heat flow to the reference (high-purity annealed aluminum) relative to the samples, was recorded as a function of temperature. Potentiodynamic polarization was carried out by using a computer controlled Meinsberger potentiostat/galvanostat with in-built PS6 software.

*PHILIPS is a trademark of Philips Electronic Instruments Corp., Mahwah, NJ.

Table I. Chemical Composition (Weight Percent) of the 8090 Alloy

Alloy	Li	Cu	Mg	Zr	Fe	Si	Al
8090	2.29	1.24	0.82	0.12	0.09	0.044	balance

III. RESULTS AND DISCUSSION

A. *Hardness Measurement and Tensile Testing*

Figure 1 shows the variation of hardness *vs* retrogression time at retrogression temperatures of 250 °C, 265 °C, and 280 °C. The graphs exhibit the characteristic behavior of

Table II. RRA Schedule Applied to Al-Li-Cu-Mg-Zr Alloy

Samples for Studies	Retrogression Temperature and Time	Reaging Schedule	RRA Temper Designation
Hardness	at 250 °C and 280 °C for 1 to 40 min	isothermal reaging (IA) at 170 °C for 2, 24, and 96 h corresponding to underaging, peak aging, and over aging tempers, respectively	—
Specimens for tensile testing, XRD, TEM, DSC and electrochemical polarization studies	at 250 °C for 12 min	IA at 170 °C for 24 h	8090R250IA
		duplex aging (DA) at 150 °C for 36 h, followed by heating to 195 °C at a rate of 5 °C/min to 7 °C/min and holding for 1 h at the temperature	8090R250DA
	at 280 °C for 8 min	IA at 170 °C for 24 h	8090R280IA
		DA at 150 °C for 36 h, followed by heating to 195 °C at rate of 5 °C/min to 7 °C/min and holding for 1 h at the temperature	8090R280DA

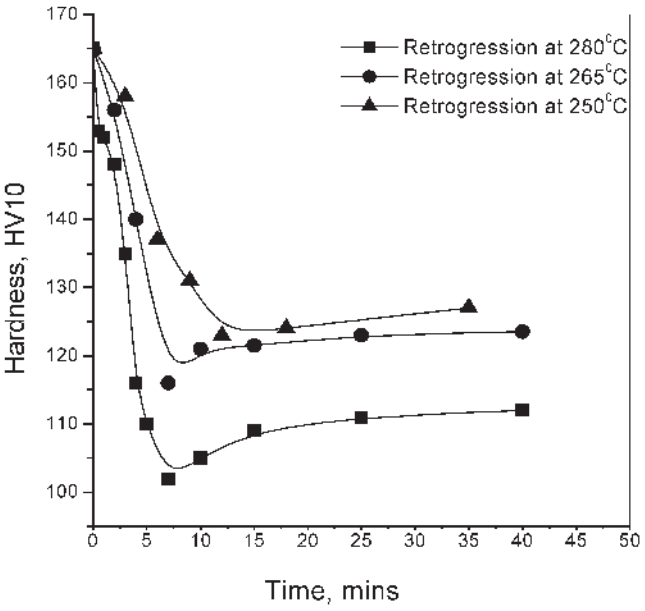

Fig. 1—Variation of hardness with retrogression time of 8090-T8 at different retrogression temperatures.

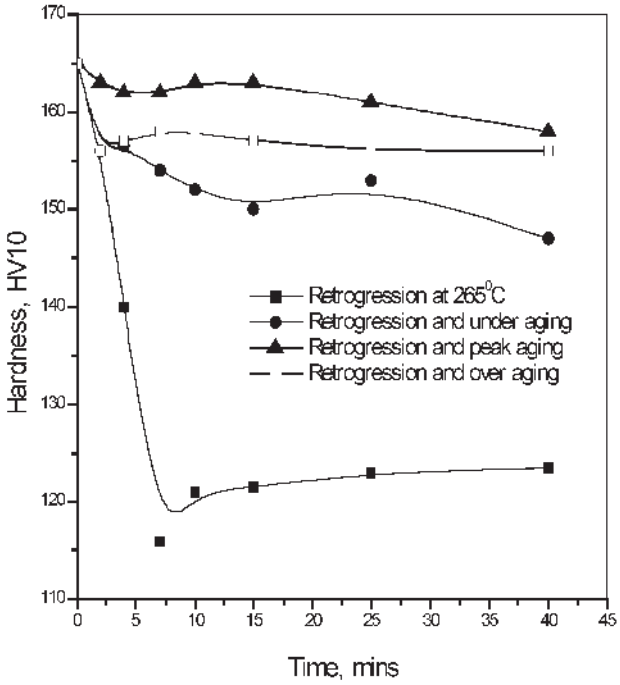

Fig. 2—Variation of hardness with time for retrogression at 265 °C and reaging to various tempers.

the retrogression phenomenon.[12,15,25] The hardness *vs* retrogression time curves have two distinct regions. These are an initial sharp decrease in hardness, attainment of minimum followed by a slight increase in hardness after which no further change in hardness values for the maximum retrogression time was studied. Further, the curves show that the higher the retrogression temperature, the greater the drop in hardness and the less the retrogression time for the minimum hardness. The trends of the results are in conformity with the results for 7xxx and 8xxx alloy series, obtained by other researchers.[18,19,21,26] Figure 2 exhibits the variation of hardness with retrogression time at a retrogression temperature of 265 °C and also the change in hardness on subsequent reaging of the retrogressed state to under-, peak-, and overaged tempers. The figures indicate that reaging the retrogressed temper causes regaining of the original peak hardness values. However, at the higher retrogression time, reaging even to the peak-aged temper failed to achieve the original peak-aged hardness values. This is due to the fact that the retrogression temperature is quite high compared to that of the artificial peak aging temperature of 170 °C; a longer retrogression time at the retrogression temperature leads to an overaging temper. The hardness values of retrogression underaged temper are lower than the hardness values of the retrogression overaged temper that are, also lower than those of the retrogression peak-aged temper. Other researchers[14,17] have observed similar trends in aluminum-base alloys.

Figure 3 shows representative stress-strain curves of the 8090 alloy of various tempers tested in universal testing machine at a crosshead speed of 2 mm/min in air. Tests were repeated to confirm the results. The strength values of the peak-aged tempers for the alloy are in conformity with those for the corresponding tempers reported in literature.[1,17,31] Further, Figure 3 indicates that the retrogression tempers have lower yield and ultimate strength values compared to those of the as-received peak-aged (T8) and retrogressed and peak-aged (RPA) tempers, but the ductility values are slightly higher.

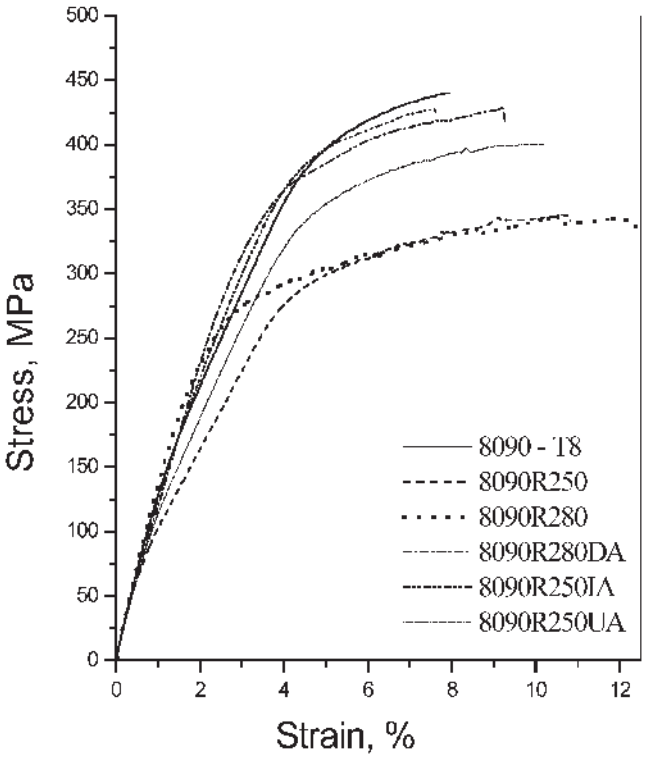

Fig. 3—Stress-strain curves of the 8090 alloy of various tempers.

The higher the retrogression temperature, the greater is the decrease in strength values and the greater is the ductility. The strength values of the retrogressed and underaged (RUA) tempers are higher than the values of the retrogressed tempers but are lower than the values in the peak-aged (T8) and RPA

tempers. The strength values of the RPA tempers are in close proximity to those of the as-received T8 temper. It is of particular interest that although the total aging time of the RRA tempers is almost twice the aging time of the conventional peak-aged (T8) temper, the yield strength and ultimate tensile strength values are in the same range of those in the conventional peak-aged (T8) temper.

The initial decrease of hardness with retrogression time is due to the preferential dissolution of the shearable coherent matrix strengthening δ' precipitates, which are no longer stable at the retrogression temperature, because the retrogression temperature is near or above the δ' solvus line.[29] However, during retrogression, other precipitates such as T_1, S', and S remain mostly undissolved.[32] However, the growth of the precipitates, particularly, S', T_1, and δ can occur to some extent[33] (Figures 8 and 9). The decrease of hardness and strength values on retrogression may also be due to the decrease of dislocation density,[16,17] as evidenced in Figure 6(b). The decrease of hardness and strength values with an increase of retrogression temperatures (Figures 1 and 3) can be attributed to the fact that higher retrogression temperature causes more dissolution of the δ' precipitates into the solution. The minima in the retrogression curves are indicative of the maximum dissolution of the δ' precipitates for the corresponding retrogression temperature. The retrogression process beyond the time corresponding to the minimum hardness will not cause further decrease of hardness, because complete dissolution of δ' precipitates is not possible upon retrogression; instead, there can be slight hardening owing to the onset of structural age hardening, *e.g.,* nucleation and growth of a new stable phase, as reported in the literature.[18,19] The present results confirm the findings of Rajan *et al.*[15] and Thakur and Balasubramaniam[17] that initially the dissolution rate is greater than the precipitation rate, but beyond a critical point, the precipitation rate of the δ' precipitates might be occurring at the same rate and thereafter the hardness remains more or less the same with retrogression time.

Reaging to retrogressed tempers causes reprecipitation of the matrix strengthening δ' precipitates resulting in an increase of hardness and strength values. Reaging the RPA temper causes complete reprecipitation of the matrix strengthening δ' precipitates, and hence, the strength properties of the RPA tempers are close to those of the T8 temper. Reaging to underaged temper causes only partial reprecipitation of the δ' phase. So, the strength values of the RUA tempers are higher than the strength values of the retrogressed tempers, but lower than the strength values of the peak-aged tempers. The lower hardness values of the retrogressed and overaged temper to that of the RPA temper are a result of the fact that overaging results in the growth of δ' precipitates.

The TEM studies have been carried out to observe the δ' precipitates in the conventional T8, retrogressed, and RRA tempers of the alloy. The TEM studies revealed that the conventional T8 and RRA tempers contain δ' precipitates, an average area fraction of 27 pct which was determined from the dark-field micrograph with the help of Leica Qwin image analysis software. However, in the retrogression state, no dark-field image of the δ' precipitates could be obtained because superlattice spots that would arise from the δ' precipitates were absent. This reflects that retrogression treatments caused dissolution of matrix strengthening δ' precipitates into solution. The TEM studies on microstructural changes associated with δ', δ, T_1, S', β' phases, dislocation densities, generation of more dislocation loops, helices, *etc.* upon RRA treatment given to this alloy have been discussed in detail elsewhere.[34]

The presence of ordered coherent shearable δ' precipitates leads to inhomogeneous slip, thereby causing severe strain localization during deformation.[1] Hence, there is limited ductility in the peak-aged tempers. Thus, in the retrogressed state, the absence of (or the presence of a very low volume fraction) of δ' precipitates and the lower dislocation density do not cause any strain localization during deformation. This results in slip homogenization contributing to an improvement of the ductility value. The homogeneous distribution of S' throughout the matrix (Figure 6(d)) minimizes coarse planar slip by promoting cross-slip and, in turn, homogenizes deformation causing an improvement of the ductility value.[33]

B. *SEM Fractography*

Figures 4(a) through (d) show some representative scanning electron fractographs of the tensile specimens of as-received peak-aged (T8), retrogressed at the temperatures of 280 °C and 250 °C and RRA tempers. The fractography reveals (1) cracking along grain boundaries or intergranular failure, (2) intersubgranular failure along the subgrain boundaries, and (3) transgranular shear failure, *i.e.,* an overall mixed mode–type fracture.

In the as-received peak-aged and RRA peak-aged tempers, fracture surfaces show a fibrous appearance, characteristic of the materials that possess a highly directional pancake-type grain structure, a type of fracture known as flutting, indicating that the final fracture has a transgranular character.[35] Laminar cracks are observed separating the transgranular and intergranular regions and extending down the fracture surface parallel to the loading direction. The spacing between the laminar cracks is associated with fracture along the grain boundaries. The lateral separation of the grains has apparently occurred due to (1) cracking along the recrystalized and unrecrystallized grain boundaries and (2) cracking along the individual subgains.

In the peak-aged (T8) and RRA temper conditions, the presence of coherent shearable δ' precipitates leads to inhomogeneous slip causing severe strain localization during deformation. This strain localization arises because of the interaction of mobile dislocations with the ordered coherent and partially coherent particles dispersed in the matrix. The strain localization due to concentrated deformation in planar slip bands and at the point of their impingement on grain boundaries is one of the reasons for crack initiation. The mechanism of intergranular cracking in 8090 alloy has been discussed by Srivatsan and Place[35] and in the T8 and RRA tempers by Lavernia *et al.*[36] in detail. Void initiation results at the intersection of a slip band and coarse grain boundary precipitates. The applied stress assists in the growth of voids. Linking of similar voids is an additional factor that promotes or enhances intergranular fracture.

Fracture surfaces of specimens with only retrogression treatments (Figures 4(b) and (c)) also exhibit mixed mode fracture. Intergranular cracking and dimples are seen. The proportion of dimples and their sizes, however, are greater than those seen in the fractographs of peak-aged and RRA tempers. The retrogressed state contains low dislocation density and low volume fraction of δ' precipitates. Thus, the strain localization arising due to the interaction of mobile dislocations with the δ' precipitates is less operative, accounting for higher ductil-

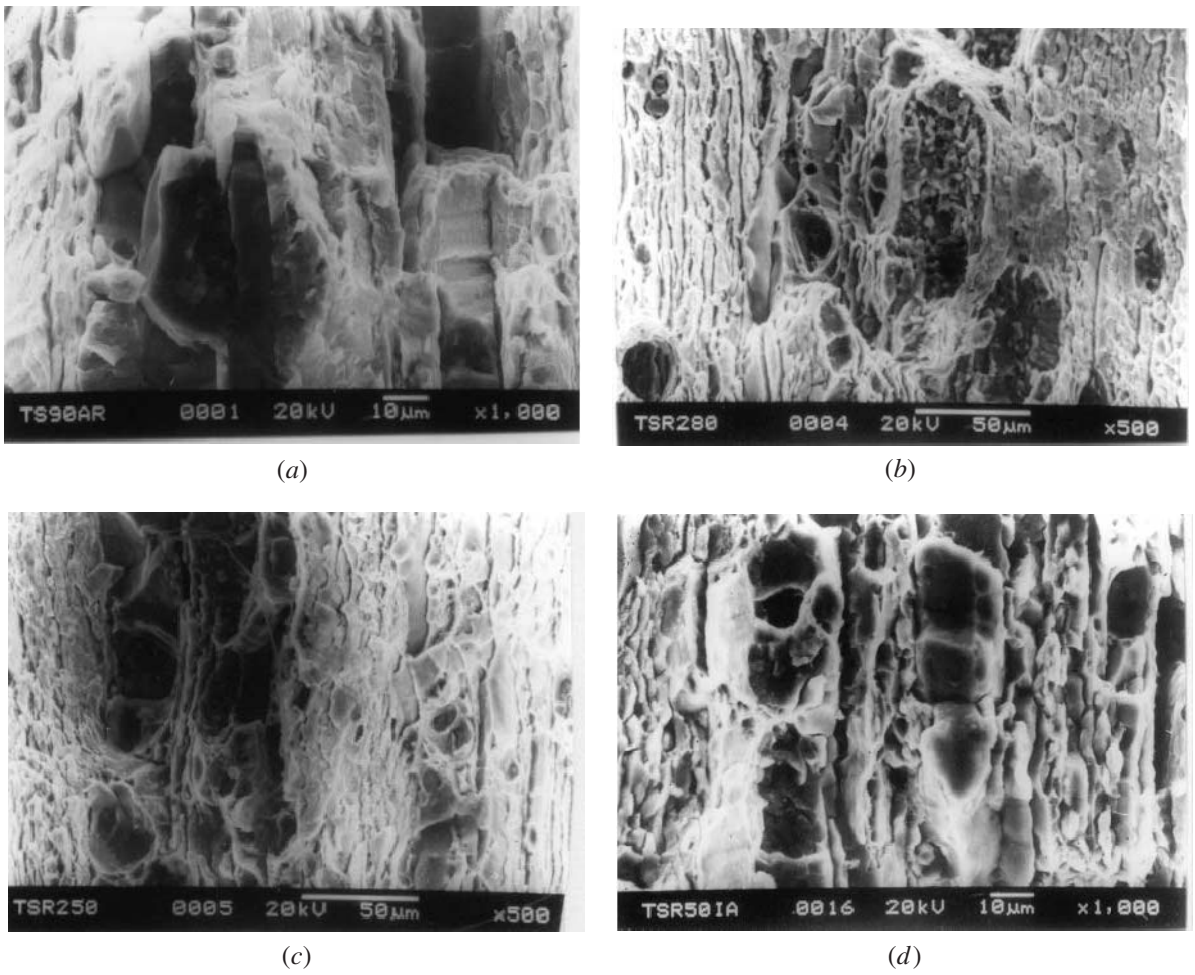

Fig. 4—SEM fractographs of (*a*) 8090-T8, (*b*) 8090R280, (*c*) 8090R250, and (*d*) 8090R250IA, exhibiting cracking along grain boundaries, intersubgranular failure along the subgrain boundaries, and transgranular shear failure, *i.e.*, overall mixed mode type fractures. Greater amounts of dimples are visible in the retrogressed states ((b) and (e)). All of the fractographs exhibit fibrous appearance, characteristic of the material of highly directional pancake-type structure.

ity in the retrogressed temper. However, the strain localization due to the presence of the grain boundary δ precipitates remains operative and hence the initiation of microvoids near the grain boundaries leads to intergranular cracking.

C. *TEM Microstructures*

Figures 5(a) and (b) shows TEM photomicrographs of 8090 alloy in the peak-aged condition, exhibiting irregular-shaped β' (Al_3Zr) dispersoids on high-angle grain boundaries as well as on the matrix, T_1(Al_2CuLi) precipitates on the matrix, and also δ (AlLi), T_1 precipitates on the grain boundaries. Diffraction patterns of the phases have not been reported, as these are well established for the alloy systems.[8,37–39] Figure 5(b) presents a dislocation structure within the grains and the subgrains of the 8090 alloy in the peak-aged T8 condition.

Figures 6(a) through (c) show TEM photomicrographs of the samples retrogressed at 280 °C followed by isothermal reaging to peak-aged temper (RRA 8090R280IA). Figure 6(a) is a dark-field image showing δ' precipitates. Figure 6(b), the TEM microphotograph of the RRA 8090R280IA tempers, shows a decrease of dislocations within the grains as compared to that in the original peak-aged T8 temper (Figure 5(b)).

Figure 6(c) shows lath-type T_1 and S′ precipitates decorated on dislocations, dislocation loops, and helices. Figure 6(d) shows TEM photomicrographs of the retrogressed and duplex-aged (8090R280DA) temper (*i.e.,* retrogressed at 280 °C followed by duplex reaging to peak-aged temper), exhibiting a uniform distribution of heterogeneous precipitation of T_1 and S′ phases within the matrix.

The β' precipitates are stable owing to the low solid solubility of Zr in Al. The dispersion of these particles, of size ranging from 20 to 30-nm diameter, is very effective in pinning grain and subgrain boundaries during thermal and mechanical processing and thus inhibiting recrystallization. On the other hand, coherent β' (Al_3Zr) precipitates provide heterogeneous nucleation sites for the matrix strengthening δ' (Al_3Li) phase. The reduction of both strain and surface energy is responsible for the effectiveness of the β' particles in nucleating δ' phase. The tendency of the dislocations to form loops on the RRA-treated samples in aluminum-base alloys has been reported.[34,40]

During retrogression, concentration of lithium atoms in the solid solution increases due to the dissolution of δ' (Al_3Li) precipitates, and this causes the nucleation and growth of the lithium-bearing phases such as S′, T_1, and δ phases.[33] The

(*a*)

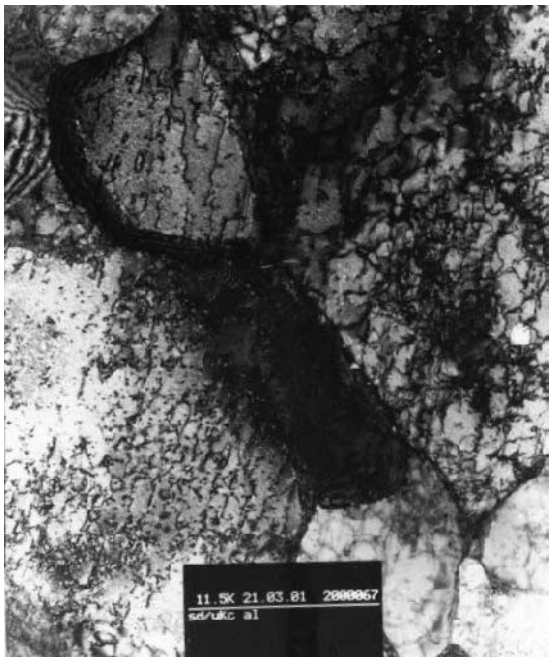

(*b*)

Fig. 5—TEM photomicrographs of the 8090-T8 temper (*a*) exhibiting β' precipitates along the grain boundaries as well as within the grains. Equilibrium δ precipitates are also visible at the grain boundaries. (*b*) Dislocation densities.

dissolution of δ' precipitates influences the vacancy concentration to the extent that vacancies are released by the dissolution of the phase. Like Mg, Li-vacancy binding energy in binary Al-Li alloy and ternary Al-Li-Zn alloys[41] has been reported to be high. Gregson *et al.*[10] claim that Li in solid solution in Al-Li-Cu-Mg alloys significantly reduces the free vacancy concentration due to its high vacancy binding energy, and that the precipitation and growth of δ' would, therefore, increase the concentration of free vacancies. This argument appears to contradict the hypothesis of Baumann and Williams[42] and of Suzuki *et al.,*[43] who maintain that the δ' phase acts as vacancy traps and confines them during aging. In the retrogression process, vacancy mobility will be affected by the increased solute content, Li, Mg, and Cu, in the solid solution, resulting from the complete dissolution of the Guinier–Preston zones and δ precipitates, as well as by the increase of temperature from ambient to retrogression (*i.e.,* 250 °C and 280 °C). Although these solute elements in solid solution are very effective in keeping vacancies bound at room temperature, they are not as effective at these higher retrogression temperatures and a percentage of these vacancies will migrate to sinks such as grain boundaries and dislocations. Some of the vacancies can collapse into loops and helices and condense on existing loops and helices. These will have an impact on the distribution of precipitates by providing nucleation sites for strengthening phases upon further artificial aging. Artificial reaging of the retrogressed state results in the reprecipitation and growth of δ' phase. With the progress of reaging time, the solid solution (*i.e.,* matrix) becomes progressively diluted in Li, thereby enhancing further the vacancy mobility and lowering vacancy supersaturation. These vacancies can continue to form loops, migrate to dislocations and form helices, or annihilate at grain boundary sinks. The first two mechanisms provide additional nucleation sites for the strengthening phases within the matrix, while the third one provides transport of solute atoms to grain and subgrain boundaries, thereby encouraging growth of S′ and T_1 at these sites.[40]

Figure 6(d), a TEM microphotograph of 8090R280DA RRA temper, exhibiting uniform precipitation of S′ and T_1 in the matrix, needs some explanation. The RRA treatments have caused an increase of T_1 phase, which has also been reflected in the X-ray diffractograms in Figures 7 and 8. This happens because, as stated earlier, during retrogression, Li goes into solution, causing growth of Li bearing phases such as T_1 and δ phases. The RRA treatments may also cause further S′ phase precipitation.[33,38] Precipitation of S′ phase in 8090 alloy depends upon free vacancy concentration, and this is a function of both solution treatment temperature and low-temperature aging, before artificial aging at a higher temperature. During reaging of the retrogressed state at somewhat low temperature (150 °C), nucleation and growth of δ' particles occur. During the growth of δ' phase, excess Cu and Mg concentration occurs at the growth front and also the vacancies strongly bound to Li atoms are released. These result in favorable conditions for the precipitation of S′ precipitates.[44] The uniform distribution of T_1 on the matrix decreases the tendency of intergranular attack, resulting in an improvement of SCC resistance,[24,45,46] while the uniform distribution of S′ phase causes an improvement of ductility by better slip homogenization.[1,37]

The lower amount of dislocation density in the RRA temper compared to that in the T8 temper (Figures 5(b) and 6(b)) is due to the fact that retrogression at a temperature of 280 °C of the peak-aged alloy causes annihilation of dislocations. Similar observations are also reported in the literature regarding the aluminum-base alloys.[16,17,34]

In the RRA tempers, the total aging time is twice the aging time of the conventional peak aging temper, and thus, the microstructure of the RRA tempers in terms of grain and subgrain boundary precipitation approaches the microstructure of

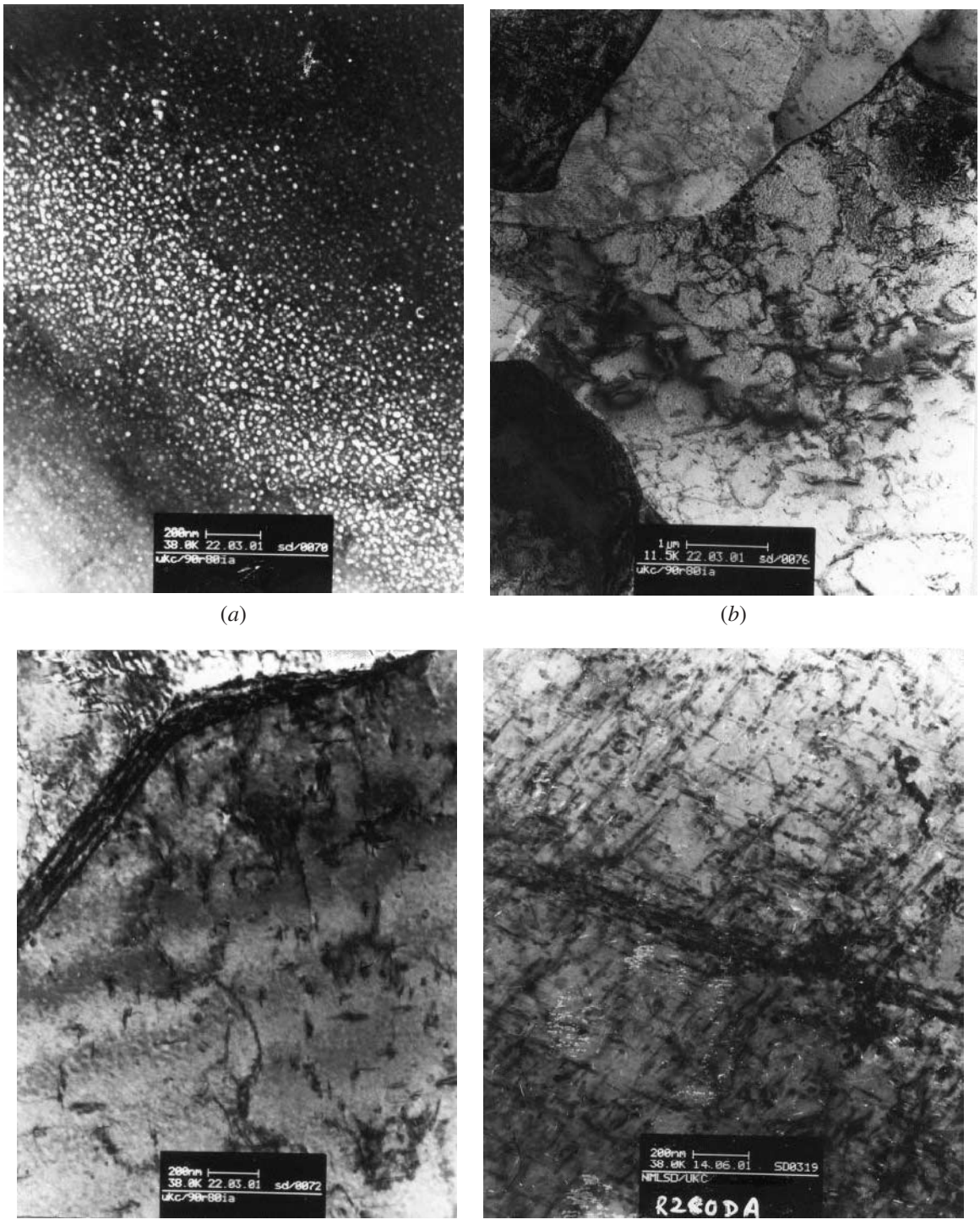

(*a*) (*b*)

(*c*) (*d*)

Fig. 6—TEM photographs (*a*) through (*c*) for the 8090R280IA temper showing (a) a dark-field image of δ' precipitates, (b) dislocation densities, (c) decoration of T_1 and S' phases on the dislocation loops and helices, and (*d*) for the 8090R280DA temper exhibiting uniform and homogeneous distribution of T_1 and S' precipitates within the matrix.

the overaging temper. The greater the aging time, the greater the δ phase precipitation on high-angle grain boundaries as well as on low-angle boundaries.[47,48] Further, during retrogression, dissolution of δ' phase increases lithium concentration in the solution and this in turn will cause nucleation and growth of the Li bearing phase. This additional δ precipitation and its growth on the grain and subgrains play an important role in imparting resistance to intergranular corrosion and stress corrosion cracking (SCC).[24,27,28,46]

D. *XRD Studies*

From the TEM micrographs, it is difficult to estimate accurately how retrogression and reaging treatments have influence

on the amount and the distribution of T_1 and S' phases individually, because of partial overlapping of the T_1 and S' phases in the microstructures. However, the XRD studies indicate the effect of RRA treatments in the precipitation of T_1 and δ phases. The effects of retrogression treatments on the S' phase precipitation could not be explained with the XRD studies, because the peaks of $Al_{(111)}$ and $Al_{(200)}$ overlap the S' phase peaks. So, for that matter, TEM and DSC studies might be helpful.

Figure 7 shows diffractograms of the 8090 Al-Li alloy at the peak-aged temper, retrogressed at the temperature 250 °C for 5 and 12 minutes, and retrogressed and peak aged (isothermal and duplex) tempers, using Co K_α radiation, whereas Figure 8 shows diffractograms of 8090 Al-Li alloy at the peak-aged temper, retrogressed at temperatures of 250 °C and peak aged temper, retrogressed at the temperature 280 °C and peak-aged temper, and overaged temper, using Cu K_α radiation.

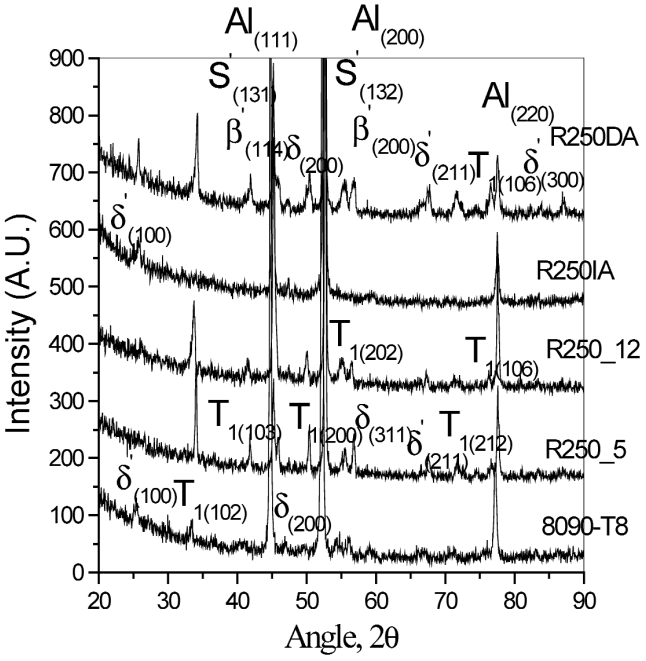

Fig. 7—XRD of the 8090 alloy of various tempers using Co K_α radiation.

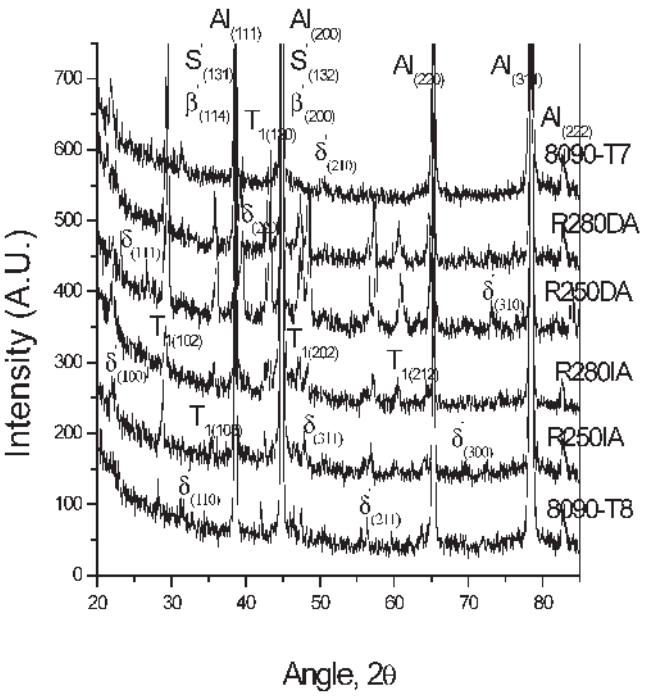

Fig. 8—XRD of the 8090 alloy of various tempers using Cu K_α radiation.

The diffractograms of all the tempers of the alloy show the peaks of all the probable phases, such as α-Al matrix, δ' (Al_3Li), δ (AlLi), S' (Al_2CuMg), T_1(Al_2CuLi), and β' (Al_3Zr), that would be present in the alloy system.[26] The diffractograms of the samples of the 8090 alloy retrogressed at 250 °C for 5 and 12 minutes exhibit the disappearance of $\delta'_{(100)}$ peak and the appearance of additional $T_{1(102)}$ peak and other intensified peaks of the T_1 and δ phases. The disappearance of the $\delta'_{(100)}$ peak is attributed to the dissolution of δ' phase in the solid solution because the retrogression temperature is above the δ' solvus line. The appearance of additional $T_{1(102)}$ peak and other intensified peaks of the T_1 and δ phases is due to the fact that as δ' phase dissolves in solution during retrogression, the lithium content of the solid solution increases and lithium bearing phases, such as δ, and T_1, nucleate and grow.

The diffractograms of the retrogressed to RRA tempers show the reappearance of the $\delta'_{(100)}$ peak with the presence of other additional peaks of T_1 and δ phases formed during retrogression. Reaging the retrogressed state to the peak-aged tempers brings back the δ' phase into the matrix, which is reflected in the diffractograms of the RRA tempers. However, once the additional peaks and intensified peaks of particular phases appear in the diffractograms of the retrogressed state, they remain as it is or they grow during reaging to peak-aged tempers.

E. *DSC Studies*

Differential scanning calorimetric studies provide complementary information on phase transformation in addition to that obtained by means of other metallurgical techniques. In particular, precipitated particles or zones can be detected by their dissolution peaks during temperature scanning even if their sizes are not large enough for an easy TEM characterization.

Figure 9 shows a DSC thermogram of solution-treated and water-quenched 8090 Al-Li alloy at a heating rate of

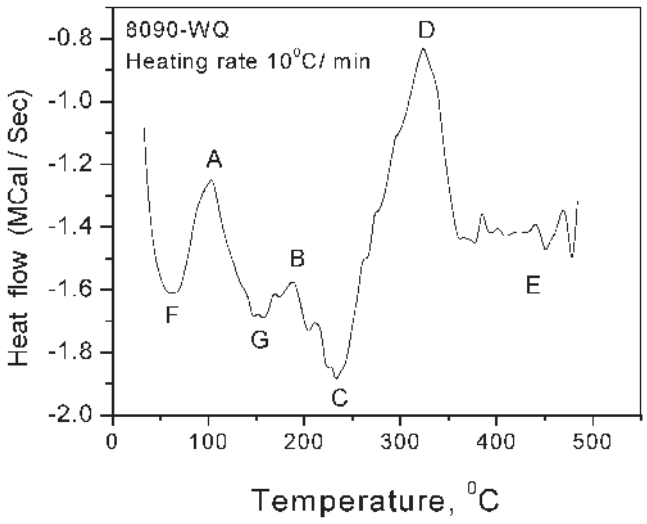

Fig. 9—DSC thermogram of solution-treated and water-quenched 8090 alloy.

10 °C/min. Figures 10(a) through (d) show the DSC thermograms of the T8 temper, retrogressed at 280 °C, retrogressed isothermal and duplex peak-aged (RPA) tempers. The curves are smoothed with the help of in-built software in the computer-controlled DSC unit, but no baseline correction is incorporated.

The thermogram in Figure 9 exhibits many exothermic and endothermic peaks (marked "A" through "G"), indicating the sequence of precipitation and dissolution reactions.[49,50,51] The precipitation reactions are as follows: A—GPB zone formation; B—precipitation of the δ' phase; C—dissolution of GPB and δ' precipitates; D—precipitation of S (S′), T_1, and δ phases; E—dissolution of S (S′), T_1, and δ phases; F—dissolution of Li-bearing zones; and G—partial dissolution of GPB zones. The precipitation and dissolution reaction kinetics of all of the phases occurring in the 8090 alloy system are discussed and analyzed in detail elsewhere.[49]

The DSC thermogram, in Figure 10(a), has two clear endothermic peak regions, C and E, and one exothermic peak region, D. The absence and/or less prominent, or minutely resolved lower temperature exotherms, *i.e.,* peaks A and B in the peak-aged tempers, indicates that the alloy is not supersaturated with solute atoms as in the as-quenched state. In other words, this alloy being in the peak-aged temper contains a maximum amount of δ' precipitates in the matrix. However, the DSC thermogram (Figure 10(b)) of the retrogressed (8090R280) state shows that the lower temperature exotherms, *i.e.,* peak regions A and B, reappear in the retrogressed temper. In the retrogressed temper, the solid solution again is supersaturated with Li atoms because of the dissolution of δ' precipitates into solution upon retrogression treatment. Therefore, during DSC runs, the reappearance of peak A (formation of GPB zones) and peak B (precipitation of δ' phase) is obvious. Figures 10(c) and (d), the DSC thermograms of the retrogressed and isothermal peak and duplex-aged tem-

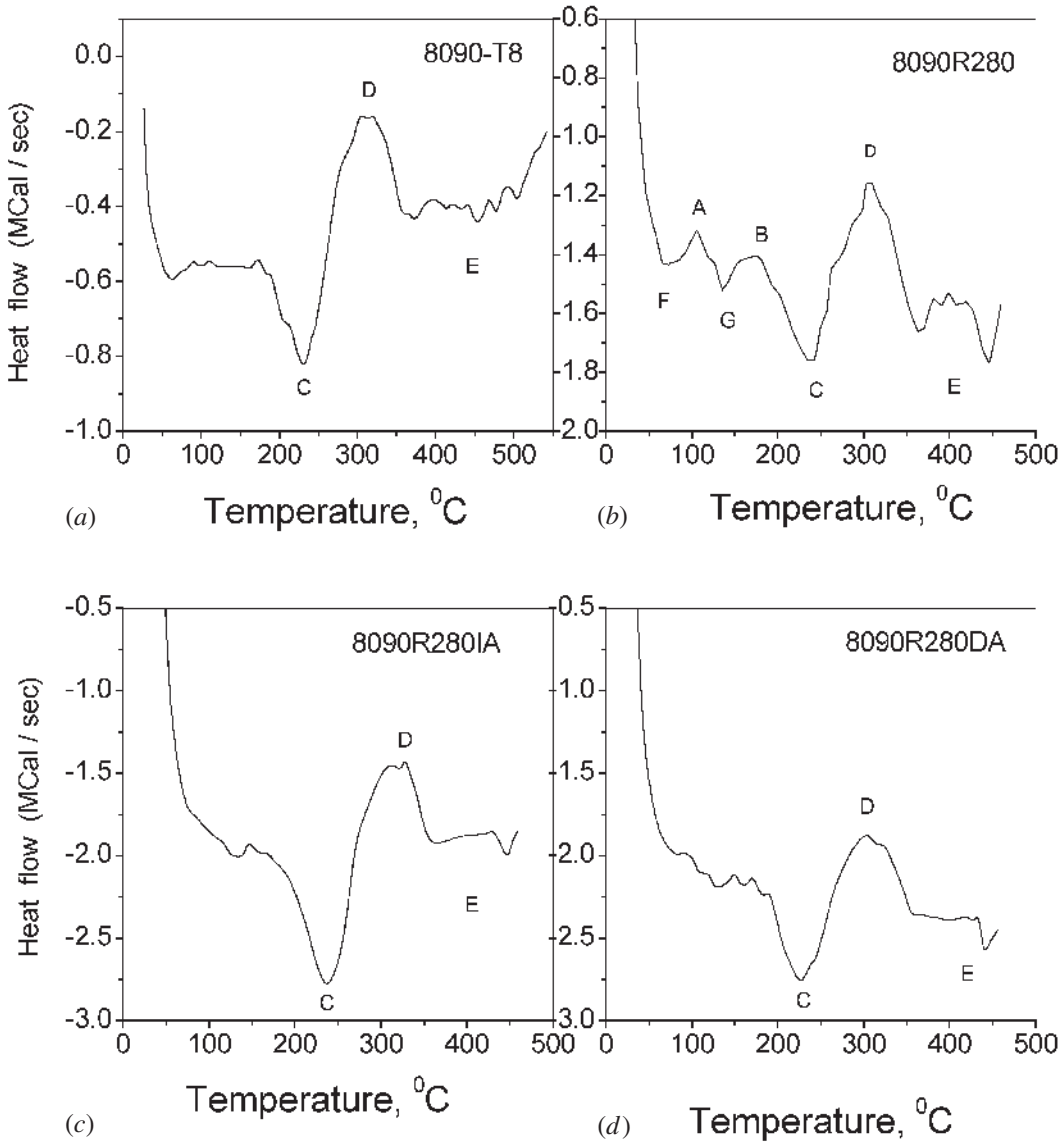

Fig. 10—DSC thermograms of (*a*) 8090-T8, (*b*) 8090R280, (*c*) 8090R280IA, and (*d*) 8090R280DA tempers at a heating rate of 10 °C/min.

pers, again show peaks C through E, similar to those of the as-received peak-aged temper. Again, the absence of lower temperature peak A and peak B indicates that the solid solution is no longer supersatutared with solutes or does contain equilibrium solute content. Thus, it can be inferred that reaging the retrogressed tempers causes reprecipitation of δ' in the matrix with additional microstructural changes.

F. *Electrochemical Behavior*

Figure 11 shows potentidynamic polarization curves of 8090 alloy in as-received peak-aged (T8), RRA, and overaged (T7) tempers in 3.5 pct NaCl solution. The shape of the polarization curves is similar for all the tempers in all environments. The curves show that the open circuit potential (OCP) values have shifted to more negative potential with aging time. Similar observations have been reported by other researchers.[46,47,52] The OCP of the overaged temper has the most negative value, whereas the OCP values of the RRA tempers lie in between the OCP values of the overaged and peak-aged tempers.

It is an established fact that the OCP depends, for a given environment, on the microstructure and the constituent phases. Thus, the shifting of OCP values in the RRA temper and with the aging time toward a more negative direction compared to the peak-aged temper is an indication of the presence of a higher proportion of anodic δ, T_1, and S' (S) phases. The negative shift in potential can also be attributed to a gradual establishment of microscopic galvanic local cell formation. The greater the aging time, the greater is the precipitation of T_1 and δ inside the grains, on the grain boundaries, as well as on the subgrain boundaries, providing sites for local cell formation. Hence based on the OCP values, it can be inferred that the microstructure of the RRA tempers approaches the microstructure of the overaged temper.

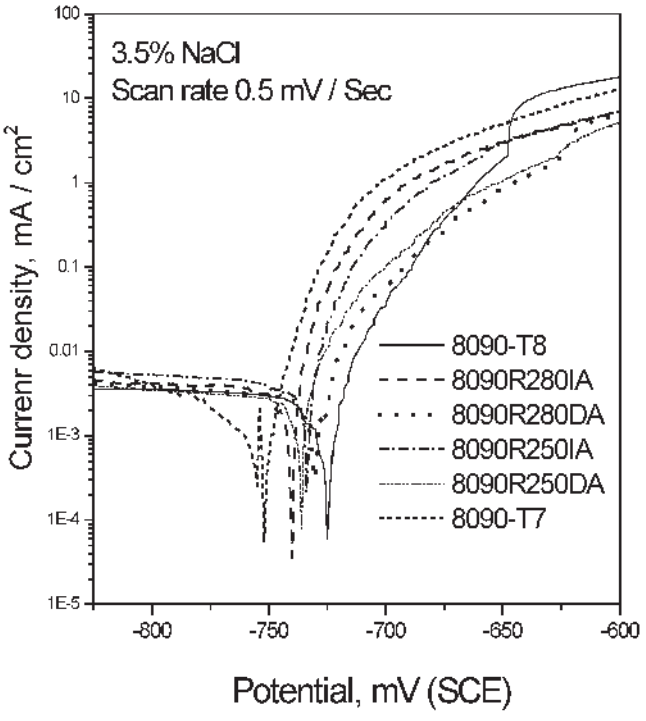

Fig. 11—Potentiodynamic polarization curves of 8090 alloy of various tempers in 3.5 pct NaCl solution.

IV. CONCLUSIONS

The TEM, XRD, and DSC studies on the 8090 alloy have revealed the presence of all of the probable phases, such as α-Al matrix, δ' (Al_3Li), δ (AlLi), S' (Al_2CuMg), T_1(Al_2CuLi), and β' (Al_3Zr) phases, that would be present in the alloy system. The XRD, TEM, and DSC studies have shown that retrogression causes dissolution of δ' phase into solid solution and reaging the retrogressed state causes reprecipitation of δ' phase in the matrix. Further, XRD studies have exhibited an additional peak and or intense peaks of T_1 and δ phases in the RRA-treated samples. The TEM studies have shown that retrogression treatment has led to a decrease of dislocation densities and the tendency of formation of loops and helices.

Retrogression treatment causes a decrease of hardness and tensile strength and an increase of ductility, which is attributed to the dissolution of matrix strengthening δ' precipitates into solution and reduction in dislocation densities. Reaging the retrogressed state leads to the reprecipitation of δ' phase within the matrix, resulting in the restoration of the original peak aged hardness and tensile strength. Fractographs of the 8090 alloy specimens of the conventional peak-aged, retrogressed, and RRA aged tempers exhibit an overall mixed mode type fracture. The fractographs of the retrogressed state also show mixed mode fracture, but the number of dimples and their sizes are more.

The OCP values of the RRA tempers lie in between the OCP values of the peak-aged and overaged tempers. The shifting of OCP values toward more negative (anodic) direction with RRA treatment and with the aging time is due to precipitation of a higher amount of anodic phases such as δ on the grain and subgrain boundaries and T_1 and S' on the matrix with overaging and RRA tempers.

ACKNOWLEGMENTS

The authors thank Drs. A.A. Gokhale and Vijaya Singh, Scientists, Defence Metallurgical Research Laboratory (DMRL, Hyderabad, India) for providing the alloy. The authors are thankful to Dr. Vikash Kumar Saxena, Scientist, DMRL, for his suggestion. Thanks are due to Mr. Samar Das, National Metallurgical Laboratory (Jamshedpur, India) for carrying out the TEM work.

REFERENCES

1. ASM Specialty Handbook, *Aluminum and Aluminum Alloys,* J.R. Davis, ed., ASM INTERNATIONAL, The Materials Information Society, Materials Park, OH, 1998, pp. 121-42.
2. M. Ahmad and T. Ericsson: *Aluminum Lithium III,* Proc. 3rd Int. Conf. on Aluminum Lithium Alloys, C. Baker, P.J. Gregson, S.J. Harris, and C.J. Peel, eds., The Institute of Metals, London, 1986, pp. 509-15.
3. J.R. Pickers, F.H. Heubaum, T.J. Langan, and L.S. Kramer: *Aluminum Lithium V,* Proc. 5th Int. Aluminum Lithium Conf., T.H. Sanders, Jr. and E.A. Starke, Jr., eds., Materials and Component Engineering Publications (MCEP), Warrendale, PA, 1989, pp. 1397-414.
4. N.J.H. Holroyd, A Gray, G.M. Scamans, and R. Hermann: *Aluminum Lithium III,* Proc. 3rd Int. Conf. on Aluminum Lithium Alloys, C. Baker, P.J. Gregson, S.J. Harris, and C.J. Peel, eds., The Institute of Metals, London, 1986, pp. 310-20.
5. F. Binsfeld, M. Habashi, J. Galland, J.P. Fidelle, D. Minnay, and P. Rofidal: *Aluminum Lithium IV,* Proc. 4th Int. Aluminum Lithium Conf., G. Champier, B. Dubost, D. Miannay, and L. Sabetay, eds., *J. Phys., Paris,* Suppl. 1987, vol. 48, pp. C3:587-C3:96.

6. B. Cina: U.S. Patent No. 3,856,584, Dec. 24, 1974.
7. B. Cina and B. Ranish: Paper No. XXV, Aluminium Industrial Products, ASM, Pittsburgh, PA, Oct. 1974.
8. P.J. Gregson and H.M. Flower: *J. Mater Sci. Lett.,* 1984, vol. 3, pp. 829-34.
9. P.J. Gregson and H.M. Flower: *Proc. Int. Conf. on Aluminium Technology '86,* T. Sheppard, ed., The Institute of Metals, London, 1986, pp. 423-28.
10. P.J. Gregson, H.M. Flower, C.N.J. Tite, and A.K. Mukhopadhyay: *Mater. Sci. Technol.,* 1986, vol. 2, pp. 349-53.
11. W.S. Miller, J. White, and D.J. Lloyd: *Aluminum Lithium IV,* Proc. 4th Int. Aluminum Lithium Conf., G. Champier, B. Dubost, D. Miannay, and L. Sabetay, eds., *J. Phys., Paris,* Suppl. 1987, vol. 48, pp. C3:131-C3:49.
12. K. Ural: *J. Mater. Sci. Lett.,* 1994, vol. 13, pp. 383-85.
13. Nguyen Cong Danh, Krishna Rajan, and W. Wallace: *Metall. Trans. A,* 1983, vol. 14A pp. 1843-50.
14. M. Kanno, I. Araki, and Q. Cui: *Mater. Sci. Technol.,* 1994, vol. 10, pp. 599-603.
15. K. Rajan, W. Wallace, and J.C. Beddoes: *J. Mater. Sci.,* 1982, vol. 17, pp. 2817-24.
16. M. Talianker and B. Cina: *Metall. Trans. A,* 1989, vol. 20A, pp. 2087-92.
17. C. Thakur and R. Balasubramaniam: *Acta Mater.,* 1997, vol. 45, pp. 1323-32.
18. J.K. Park: *Mater. Sci. Eng.,* 1988, vol. A103, pp. 223-31.
19. Matthew B. Hall and John W. Martin: *Z. Metallkd,* 1994, vol. 85, pp. 134-39.
20. M.U. Islam and W. Wallace: *Met. Technol.,* 1983, vol. 10, pp. 386-92.
21. M.U. Islam and W. Wallace: *Met. Technol.,* 1984, vol. 11, pp. 320-22.
22. B.S. Kaneko: *Met. Progr.,* 1980, vol. 11, pp. 41-43.
23. J.S. Robinson: *Mater. Sci. Forum,* 2000, vols. 331–337, pp. 1653-58.
24. A. Gray, N.J.H. Holroyd, and J. White: *Aluminum Lithium V,* Proc. 5th Int. Aluminum Lithium Conf., T.H. Sanders, Jr. and E.A. Starke, Jr., eds., Materials and Component Engineering Publications (MCEP), Warrendale, PA, 1989, pp. 1175-86.
25. V. Komisarov, M. Tlianker, and B. Cina: *Mater. Sci. Eng.,* 1996, vol. A221, pp. 113-21.
26. V. Komisarov, M. Tlianker, and B. Cina: *Mater. Sci. Eng.,* 1998, vol. A242, pp. 39-49.
27. Z.Q. Hu, Y. Zhang, Y.L. Liu, and Z.Y. Zhu: *Corrosion,* 1993, vol. 49, pp. 491-98.
28. K.S. Ghosh, K. Das, and U.K. Chatterjee: *Online J. Corr. Sci. Eng.,* 2003, vol. 6, paper no. C014 (preprint available).
29. O. Jensrud and N. Ryum: *Mater. Sci. Eng.,* 1984, vol. 64, pp. 229-36.
30. S. Fox, H.M. Flower, and D.C. McDrmaid: *Aluminum Lithium III,* Proc. 3rd Int. Conf. on Aluminum Lithium Alloys, C. Baker, P.J. Gregson, S.J. Harris, and C.J. Peel, eds., The Institute of Metals, London, 1986, pp. 263-72.
31. G.M. Reddy, A.A. Gokhale, and K. Prasad Rao: *Sci. Technol. Welding Joining,* 1998, vol. 3, pp. 151-58.
32. R.E. Ricker, J.L. Fink, and A.K. Vasudevan: *Metall Trans., A* 1991, vol. 22A, pp. 264-67.
33. C.P. Blankenship, Jr. and E.A. Starke: *Metall. Trans.,* 1993, vol. 22A, pp. 833-41.
34. K.S. Ghosh, K. Das, and U.K. Chatterjee: *Mater. Sci. Technol.,* 2004, vol. 20, pp. 825-34.
35. T.S. Srivatsan and T. Allan Place: *J. Mater. Sci.,* 1989, vol. 24, pp. 1543-51.
36. I.J. Lavernia, T.S. Srivatsan, and F.A. Mohamed: *J. Mater. Sci.,* 1990, vol. 25, pp. 1137-58.
37. H.M. Flower and P.J. Gregson: *Mater. Sci. Technol.,* 1987, vol. 3, pp. 81-90.
38. R. De Jesus and A.J. Ardell: *Al-Li V,* pp. 661-76.
39. K. Satya Prasad, A.A. Golhale, A.K. Mokhopadhyay, D. Banerjee, and D.B. Goel: *Acta Mater.,* 1999, vol. 47 (8), pp. 2581-92.
40. K.S. Kumar, S.A. Brown, and J.R. Pickens: *Acta Mater.,* 1996, vol. 44, pp. 1899-915.
41. S. Caresara, A. Giarda, and A. Sanchez: *Phil. Mag.,* 1977, vol. 35, p. 97.
42. S.F. Baumann and D.B. Williams: *Metall. Trans., A* 1985, vol. 16A, pp. 1203-11.
43. H. Suzuki, M. Kanno, and N. Hayashi: *J. Jpn. Inst. Light Met.,* 1981, vol. 31, p. 122.
44. V. Radmilovic, G. Thomas, G.J. Shiflet, and E.A. Starke Jr.: *Scripta Metall.,* 1989, vol. 23, pp. 1141-146.
45. Z.F. Wang, Z.Y. Zhu, Y. Zhang, and W. Ke: *Metall. Trans. A,* 1992, vol. 23A, pp. 3337-41.
46. A. Gray: *Aluminum Lithium IV,* Proc. 4th Int. Aluminum Lithium Conf., G. Champier, B. Dubost, D. Miannay, and L. Sabetay, eds., *J. Phys., Paris,* Suppl. 1987, vol. 48, pp. C3:891-C3:904.
47. J.M. Sater and T.H. Sanders: *Aluminum Lithium V,* Proc. 5th Int. Aluminum Lithium Conf., T.H. Sanders, Jr. and E.A. Starke, Jr., eds., Materials and Component Engineering Publications (MCEP), Warrendale, PA, 1989, pp. 1217-25.
48. P. Niskanen, T.H. Sanders Jr., J.G. Rinker, and H. Marek: *Corr. Sci.,* 1982, vol. 22, pp. 283-304.
49. A. Luo, D.J. Lloyd, A. Gupta, and W.V. Youdelis: *Acta Metall. Mater.,* 1993, vol. 41, pp. 769-76.
50. M.J. Starink, A.J. Hobson, and P.J. Gregson: *Scripta Mater.,* 1996, vol. 34 (11), pp. 1711-16.
51. A.K. Mukhopadhyay, C.N.J. Tite, H.M. Flower, P.J. Gregson, and F. Sale: *Conf. Proc.,* Proc. 4th Int. Aluminum Lithium Conf., G. Champier, B. Dubost, D. Miannay, and L. Sabetay, eds., *J. Phys., Paris,* Suppl. 1987, vol. 48, pp. C3:449-C3:446.
52. M. Reboul and P Meyer: Proc. 4th Int. Aluminum Lithium Conf., G. Champier, B. Dubost, D. Miannay, and L. Sabetay, eds., *J. Phys., Paris,* Suppl. 1987, vol. 48, pp. C3:881-C3:89.